Published in final edited form as:
IEEE Trans Med Imaging. 2007 November ; 26(11): 1448–1455. doi:10.1109/TMI.2007.906787.

New Perspectives on the Sources of White Matter DTI Signal

Sharon Peled
The author is with the Harvard Center for Neurodegeneration and Repair and Brigham and Women's Hospital, Boston, MA 02115 USA (speled@bwh.harvard.edu).

Abstract

A minimalist numerical model of white matter is presented, the objective of which is to help provide a biological basis for improved diffusion tensor imaging (DTI) analysis. Water diffuses, relaxes, and exchanges in three compartments—intracellular, extracellular, and myelin sheath. Exchange between compartments is defined so as to depend on the diffusion coefficients and the compartment sizes. Based on the model, it is proposed that an additive "baseline tensor" that correlates with intraaxonal water volume be included in the computation. Anisotropy and tortuosity calculated from such analysis may correspond better to tract ultrastructure than if calculated without the baseline. According to the model, reduced extracellular volume causes increased baseline and reduced apparent diffusion. Depending on the pulse sequence, reduced permeability can cause an increase in both the baseline and apparent diffusion.

Index Terms

Brain; magnetic resonance imaging (MRI); water diffusion; white matter (WM) disease

I. INTRODUCTION

A relationship is often assumed to exist between the parameters measured from diffusion tensor imaging (DTI) in the white matter (WM) of the brain, and the tissue ultrastructure, or even its functional integrity. In many recent research studies, fibers are clustered based on their terminations or other criteria, and scalar parameters characterizing the tract, such as anisotropy or mean diffusivity, are assessed [1]–[3]. Conclusions are then drawn about structural or functional characteristics of the tract. This paper attempts to add to the quantitative theoretical basis for structural inferences, through a realistic modeling approach. This knowledge can potentially drive the choice of magnetic resonance imaging (MRI) pulse sequence, the choice of acquisition parameters, and the choice of DTI analysis method.

The factors potentially determining DTI signals in WM can be roughly divided into two groups.

1. Factors due to partial voluming within a voxel i.e., inclusion of CSF or gray matter in the voxel, or multiple tract directions within one voxel. The latter can be due to different configurations such as fanning out of fibers, crossing fibers, etc. If a voxel lies on a border of white and gray matter, the more isotropic gray matter diffusion should be taken into account. This event can be recognized e.g., by segmentation of a co-registered anatomical scan. But when a voxel lies on the intersection of two fiber bundles, no evidence of this can be found in any current imaging methodology apart from diffusion MRI. Many investigators have addressed this issue in the context of DTI, e.g., [4]–[6]. A significant improvement in the assessment of parameters such as anisotropy can be obtained just from taking into account the possibility of two fiber bundles in a voxel.

2. Factors pertaining to the microstructural tissue characteristics of coherent fiber bundles—for reviews, see [7]–[9]. These factors would include, for example, average values of axon diameters, fiber spacing, myelination percent, permeability, diffusivity, T_2 relaxation times, etc.

The effect of the latter group of tissue characteristics on the DTI signal is modeled here. This work builds on a large number of previous analytical and numerical investigations of diffusion in neural tissue, among them [10]–[17].

Early papers of particular relevance, in terms of methodology and objectives, to the current work are the theoretical studies by Szafer *et al.* [11] and by Ford *et al.* [17]. Both simulated water in tissue using Monte Carlo methods and concluded that cell swelling would affect the apparent diffusion constant. In the former, tissue was represented as a periodic array of boxes separated from an extracellular space by permeable membranes, while in the latter the cells were cylindrical. The current study includes a myelin compartment with its own water density, T_2, and diffusivity. Permeability is defined in a physically meaningful way for compartments that are not well mixed. The effects of clinically viable DTI pulse sequences are simulated resulting in a new, biologically-motivated, method of DTI analysis and interpretation.

A. Diffusion Measurement in WM

When water diffusion in myelinated neural tissue is measured by MRI, the first finding is that the signal is not a monoexponential function when plotted against b [18]. The parameter b represents the level of diffusion weighting and is a function of the applied magnetic field gradients and their temporal spacing. A monoexponential diffusion decay would be expected when a single population of spins is freely diffusing, i.e., not encountering barriers. In the case of one-dimensional free (or Gaussian) diffusion, the signal is given by $S \propto e^{-bD}$ where D is the diffusion constant. Only in the case of free (or hindered—see below) diffusion can the signal be described this way. Embedded in DTI analysis is an assumption of Gaussian diffusion. The general description for the signal attenuation in a conventional spin-echo diffusion tensor experiment, with two field gradients, **g** applied for duration δ and separated by time Δ is [19], [20]

$$S(\mathbf{g}) = S_0 e^{-\gamma^2 \delta^2 (\Delta - \delta/3) \mathbf{g}' \mathbf{D} \mathbf{g}}, \quad (1)$$

where γ is the gyromagnetic constant and **D** is the diffusion tensor.

An accepted approach to elucidation of the underpinnings of the signal is to analyze multiple b-value data, often involving bi-exponential fits to the data [21], [22]. Many authors have pointed out that the multiexponential characteristics of the diffusion curve in WM cannot be freely related to the geometrical parameters of the system. Other mechanisms for quasi-bi-exponentiality have been proposed, such as finite membrane permeability [23], and the existence of a distribution of different compartment sizes [24].

In order to illustrate the essential characteristics of diffusion-weighted data in WM and its analysis, typical diffusion curves from *in vivo* human WM are shown in Fig. 1. Midline sagittal diffusion-weighted double spin-echo echo-planar scans acquired on a 3T GE scanner were repeated for multiple b-values, ranging up to 4000 s/mm^2 (4 ms/μ^2), and for three gradient directions—two approximately perpendicular (X and Y) and one approximately parallel (Z) to the corpus callosum fiber direction, i.e., in-plane and through-plane, respectively. Data acquisition details are given here for completeness, but are peripheral to the issue at hand. Image matrix was 128 × 128 in a field-of-view of 24 cm with slice thickness 3 mm and TE 114 ms. The high b-value data was averaged up to 8 times.

Plotted in Fig. 1 is the mean image intensity of 552 voxels segmented from the corpus callosum for gradient directions parallel (green circle) and perpendicular (blue circle) to the tracts. The anisotropy of diffusion in WM—the basis of DTI—is apparent. The parallel diffusion data falls off rapidly and thus exhibits a Rician noise baseline (dotted green line is the mean of artifact-free area of background shown in red rectangle), but it can be adequately fitted by a monoexponential function (green line in Fig. 1), indicating free diffusion. However, a monoexponential fit to the perpendicular diffusion curve (dashed blue line in Fig. 1) is clearly inadequate, as is a monoexponential fit to the first 5 points (dotted blue line). A much better fit is obtained by adding a baseline term to the fitting equation (solid line). Note that the number of data points necessary for a monoexponential + baseline fit is significantly less than for a bi-exponential fit. Inadvertent deviation from an exact mid-sagittal location in this example would tend to increase the measured transverse diffusion, and decrease the measured parallel diffusion.

Two useful measures reflecting WM ultrastructure are anisotropy and extracellular tortuosity. Tortuosity indicates the change in path length due to the convoluted space of the extracellular environment. It is defined by

$$\lambda = \sqrt{\frac{D_A}{D_{\text{app}}}} \tag{2}$$

where D_A is the intrinsic diffusion constant in the extracellular space and D_{app} is the measured (apparent) diffusion [25]. The intrinsic diffusion, D_A can be measured, for example, from the parallel diffusion curve. In Section II, it will be proposed that D_{app}, the extracellular apparent diffusion, is given by the decay term in the monoexponential + baseline fit of the perpendicular diffusion. From the graph in Fig. 1, $D_A \approx 1.98\ \mu^2/\text{ms}$ and $D_{\text{app}} \approx 0.84\ \mu^2/\text{ms}$ thus in this case: $\lambda \approx \sqrt{1.98/0.84} = 1.54$. In mammalian brain λ has been estimated by non-NMR methods to be approximately 1.6 [25].

A commonly used measure for quantification of diffusion anisotropy is the fractional anisotropy (FA), introduced by Basser *et al.* [26]. The right-hand axis in Fig. 1 shows the FA that would be calculated from this data for each *b*-value, assuming only that *b*-value had been measured (in addition to $b = 0$), and the data fit to a monoexponential function. Thus, without baseline analysis, the value of FA is not constant and depends on the *b*-value at which it is measured as well as on the height of the noise baseline. The value of FA can also depend on the pulse sequence used to measure diffusion—see next subsection.

B. b-Value Determination

In the case of non-Gaussian diffusion, different gradient pulse sequences can tender the same *b*-value but effect different diffusion attenuation. For comparison one could consider a standard spin-echo diffusion measurement and a stimulated echo diffusion experiment [27]. In a stimulated echo sequence *b* values can be obtained with longer mixing times Δ and thus shorter gradient pulses are possible. This is important because when restriction is assessed by standard methods, the diffusion of restricted compartments will appear to be more restricted (smaller) the longer the gradient pulses are [28]. Longer mixing times can be beneficial when investigating slow water exchange, for example. The other pertinent differences of the stimulated echo experiment compared to the spin echo experiment are:

- the effect of T_2 relaxation is reduced, although T_1 relaxation may become a factor at very long mixing times;
- only 50% of the spin magnetization is ultimately available for measurement.

Given the longer mixing time and lower sensitivity to T_2 of the stimulated echo experiment, one would expect the specific NMR characteristics of the myelin, and the permeability, to have a larger effect on the measurements. These parameters will be explained further in Section II.

II. METHODS

A. Model Parameters

WM is a compact tissue. It is modeled here with hexagonal spacing, allowing a minimum of 9% volume for extra-cellular (EC) space when adjacent fibers abut. All the fibers are the same size. When modeling diffusion in WM, some approximations need to be made. The main assumptions of this model are presented below.

1. Three compartments exist in the tissue—intracellular (IC), myelin sheath (M), and EC. The configuration of the modeled tissue is depicted in Fig. 2. Although these three compartments are not necessarily homogeneous, and other spaces exist, for example, astrocyte cell bodies, these compartments represent the majority of volume and water content in human WM. The average EC volume fraction in whole brain is 20% [25], with the EC fraction in WM being slightly less than the average [25], [29].
2. Axons are cylindrical and myelinated (axons with diameter > 0.2 μ are generally myelinated [30]). Although approximately half of the axons in WM are in fact unmyelinated, they are very small and represent a small fraction of the MR signal.
3. In normal WM, on average, the outer diameter of the myelinated fiber, including the myelin sheath, is given by $a/0.6$ where a is the axon diameter [31].
4. All of the water is MR-visible.
5. The diffusion coefficients in EC and in IC (D_A) are set to be equal—no evidence exists to support a significant difference. The diffusion coefficient in myelin (D_B) is assumed to be lower or equal to the IC value.
6. The T_2 times in IC and EC (T_A) are assumed to be equal and to be comparable in value to that of gray matter. T_2 in the myelin compartment (T_B) is assumed to be significantly lower than in the IC compartment [32].
7. The model does not include direct water exchange between IC and EC space. This is in consideration of the relatively small surface area common to these two compartments. Exchange would occur at the nodes of Ranvier—breaks in the myelin sheath—which are spaced approximately 1 mm apart along the axon and extend over ~ 1 μ.

Some of the parameters used in the model are shown in Fig. 2.

B. Parameter Estimation

When equally sized cylinders are distributed in a hexagonal grid, with 18% extracellular space and a ratio of 0.6 for axon diameter:fiber diameter, the resulting volume of myelin is 52.5%—this was kept constant throughout the simulations. The EC fractional volume was varied between 10% and 26%, designated by the parameter α in Table I.

Given the aforementioned constraints, the dependence of the axon diameter a on EC fraction is given by

$$a = 2 \cdot \mathrm{SPC} \sqrt{\frac{(1 - \alpha - \xi)\sqrt{3}}{2\pi}} \quad (3)$$

where ξ is the myelin volume fraction (fixed here at 52.5%), and SPC is the spacing between axon centers—set here to either 3 or 6 μm.

The total water content in WM is approximately 72% [33]. The myelin sheath comprises approximately 50% of total dry weight in WM, with the myelin water content *in situ* estimated at 40% [33]. This results in an estimation that approximately 13% of the water in WM is associated with the myelin compartment. Estimations based on the decomposition of T_2 curves in MRI have yielded myelin water fractions in the range 8–15% [32].

Spin relaxation in the different cellular environments may affect DWI measurements. The T_2 of myelin-associated water has been measured to be between 10–50 ms at 1.5 T [32]. For the T_2 time in the IC and EC, the T_2 of gray matter is assumed, i.e., approximately 85 ms at 3 T [34].

There is no consensus on water exchange rates in WM. The IC residence time has been estimated at less than 15 ms [16], less than 20 ms [35], and between 370 ms & 1087 ms [36]. The compartments in WM are not well mixed, i.e., the particles close to the boundaries have a higher probability of exchange. Instead of defining a mean residence time, here permeability is defined by the fraction of particles that are allowed to exchange after colliding with the wall, designated by κ in Table I. The number of wall hits is affected by the size of the compartment and the diffusion constant. Translating this permeability parameter into a conventional exchange time is not straightforward, but can be performed at the conclusion of the simulation. The formula used here for the average residence time is

$$\tau = \frac{\mathbf{TE}}{\beta} \quad (4)$$

where β is the average number of exchanges the particles undergo in TE. Another possible measure of exchange, that emphasizes IC–EC transfer, is the percentage of particles that began in the IC compartment that ended up in the EC after TE.

C. Simulation

The diffusion equations were simulated using a Monte Carlo method. The simulated diffusion-weighted pulse sequences were a spin-echo (Δ = 40 ms, δ = 35 ms) and a stimulated echo (Δ = 245 ms, δ = 12 ms). Each simulation run calculated complex signals from 10 000 particles for 42 gradient configurations—21 perpendicular and 21 parallel to the fibers—between zero and 4 G/cm (the current maximum on standard clinical scanners). The simulation was programmed in Matlab version 7 R13 (Mathworks, Natick, MA). The run time for each one of the 400 parameter combinations in Table I was approximately 10 minutes on a dual-core AMD Opteron 880 processor, running at 2.4 Ghz with 64 GB of RAM and 750 GB of local fast file storage space.

The particles are initially distributed randomly according to compartmental densities in one hexagonal unit of the hexagonal array, with 13% placed in the myelin compartment and the remaining 87% distributed among the IC and EC according to their respective volumes. For each time step (t = 10 μs), the particles diffuse and relax: the magnitude of the magnetization is multiplied by e^{-t/T_2} according to the T_2 of the compartment, and the position is changed by $\sqrt{6Dt}$ where D is the compartmental diffusion constant. The 3-D angle of diffusion

direction is random, in spherical coordinates $\phi = 2\pi u$ and $\theta = \cos^{-1}(2v - 1)$ where u and v are uniformly distributed random variables on the interval [0,1]. If a gradient pulse is on, the phase of each spin packet changes by $\gamma \mathbf{g} \cdot \mathbf{r}$ where γ is the gyromagnetic ratio, $\mathbf{g}$ is the applied field gradient, and $\mathbf{r}$ is the location of the spin. The 180° pulse inverts all spin phases.

When a particle hits a compartment boundary, it can either transfer to the new compartment, or suffer one or more "billiard ball" reflections, traversing the remainder of its trajectory in its original compartment. The proportion of particles hitting the wall that indeed transfer, is the permeability parameter, κ, set by the experimenter. Mass is preserved in each compartment by allowing equal numbers to enter and to exit at each time step. This is accomplished as follows. In each iteration, when n particles in compartment type A hit a boundary with compartment type B, and m particles in compartment type B hit a boundary with compartment type A, the number of particles allowed to cross each way is $\lfloor \kappa \min(n, m) \rfloor$, randomly chosen from those that collided. The remainder suffer elastic collisions with the wall and stay in their original compartment. In order to accommodate situations in which very small numbers are hitting the wall or allowed to exchange (either due to low density, low diffusion, short diffusion intervals, or low permeability) the fraction $\kappa \min(n, m) - \lfloor \kappa \min(n, m) \rfloor$ is carried over and added to the number allowed to exchange in the following iteration. Over time this eliminates the rounding error and allows a smaller number of particles to be used in the simulation.

Fig. 3 shows typical plots of particle locations at the start of the simulation [Fig. 3(a)], and after 10 ms of motion and relaxation [Fig. 3(b) and (c)]. Changing the EC fraction from $\alpha = 0.26$ to $\alpha = 0.10$ causes the fibers to abut and significantly reduces the average distance traveled in 10 ms. In these particular simulated data sets, permeability is zero.

D. Analysis

When $\kappa = 0$, i.e., the permeability is zero, the measured diffusion is exactly the sum of the signals originating in each compartment. Fig. 4 shows transverse diffusion data from the simulations with $\kappa = 0$, SPC = 6 μ, $T_B = 10$ ms, $D_B = 0.5$ μ^2/ms, $\alpha = 0.18$, $TE = 75$ ms, broken down by compartment.

1. The myelin compartment spins have completely relaxed in this time, contributing virtually no signal.
2. The IC spins are so restricted and the gradient pulses are so long, that the IC diffusion signal is barely attenuated at these b-values. Therefore, the signal can be well approximated as a constant independent of b. Recently, Kroenke *et al.* have shown that the diffusion of NAA (which is localized to neuronal IC space) at $\Delta = 50$ ms in a rat brain can be fit by a model which consists of randomly oriented cylinders with zero apparent diffusion perpendicular to the cylinder axes [37]. See the Appendix for further explanations.
3. The EC spins exhibit hindered diffusion with a monoexponential decay governed by an apparent diffusion constant, D_{app}.

Thus, it is proposed that a monoexponential + constant fit should be utilized for the perpendicular diffusion. The exponent corresponds to D_{app}, and the baseline to the relative volume of IC water. Nonzero permeability is expected to affect the interpretation of the fit.

III. RESULTS

Table II shows the range of exchange times (other than $\kappa = 0$, $\tau = \infty$) covered by this simulation for a subset of tissue configurations (here, $\alpha = 0.18$ ms). The IC residence times

in this simulation are shorter or comparable to published estimates [16], [35], [36]. Shown in parentheses are values for the percent of particles that moved from IC to EC in TE = 75 ms. Interestingly, for any given permeability, κ, the residence time, τ, and the percent of spins moving from IC to EC are approximately equal for the configurations $\{D_B = 0.5\ \mu^2/\text{ms}$, SPC = 3 μ} and $\{D_B = 2\ \mu^2/\text{ms}$, SPC = 6 μ}. This suggests a dependence of residence time on SPC/$\bar{u}_B$ where $\bar{u}_B$ is the mean squared displacement in the myelin compartment. Thus, D_B may be a rate-limiting factor in IC–EC water exchange.

Fig. 5 shows simulated transverse diffusion attenuation plots for permeabilities $\kappa = 0$ and κ = 1%, and for different EC volumes, α, fitted by monoexponential functions with baselines. The data is well fitted by these functions, even in cases of high permeability. However, only when the permeability, κ, is zero, does the baseline strictly correspond in size to the axonal water fraction, and the decay constant correspond to the hindered diffusion constant.

Fig. 6(A) and (B) shows plots of the apparent diffusion and baseline computed from fits of the simulated spin-echo (Δ = 40 ms) data at different combinations of α, κ, and SPC. The line of bold ×'s in Fig. 6(B) shows the percent of the signal attributable to axonal water. To calculate the axonal water fraction, note that at time TE = 75 ms, the myelin water has relaxed and is not contributing to the signal any longer. The axonal fraction of the remaining signal is given by

$$\frac{V_{\text{IC}}}{V_{\text{IC}}+V_{\text{EC}}}=\frac{1-\xi-\alpha}{1-\xi} \tag{5}$$

where ξ is the fractional volume of the myelin sheath (here always taken as 0.525) and α is the fractional volume of EC. Clearly both the baseline and apparent diffusion (D_{app}) are highly affected by the EC volume fraction (α), the former quite linearly as is expected since in the absence of exchange it is a direct measure of the IC volume fraction. Permeability does not much affect the baseline (i.e., the IC volume fraction estimation) at this Δ, although D_{app} reduces with higher permeability. Increased fiber size, given by the spacing of the hexagonal grid, SPC, tends to increase D_{app}. For the longer diffusion time (Δ = 245 ms) of the stimulated echo experiment, higher permeability results in both a lower baseline and lower apparent diffusion, as shown in Fig. 6(C) and (D). However, a larger EC space yields a lower baseline and higher D_{app}—this difference in the effect of these two parameters may prove useful when comparing DTI tracts. The increase in apparent diffusion is greater for larger axons. The effects of increased permeability on the diffusion signal are similar to the effects of decreased axon diameter, which corresponds to the dependence of exchange on the number of wall hits.

Extracellular tortuosity can be estimated from the fitted D_A (parallel diffusion) and D_{app}, based on (2). The fitted values of D_A for the spin-echo simulation are generally in the range 1.95–2, and for the stimulated-echo experiment in the range 1.90–2, with lower values for higher permeability. Given the constancy of D_A, the apparent tortuosity here is mostly determined by D_{app}.

IV. DISCUSSION

All factors that influence the signal need to be taken into account in order to make statements about tissue ultrastructure based on DTI. Given the many simplifying assumptions that are necessary in order to create a model, the objective is not to accurately describe geometrical tissue characteristics, but to identify trends and possible biological sources for differences in tract parameters calculated from DTI.

Based on the model it is proposed that the diffusion attenuation signals $S_\perp$, $S_\parallel$ obtained with field gradients applied perpendicular and parallel respectively to a single fiber bundle with coherently organized fibers, can be described by:

$$\begin{cases} S_\perp = & S_0 \left((1 - C_0)\, e^{-bD_{\text{app}}} + C_0 \right) \\ S_\parallel = & S_0 e^{-bD_A}. \end{cases} \tag{6}$$

A monoexponential + baseline yields more information for tissue characterization than a monoexponential fit alone, and is rooted in the tissue structure. Note that only perpendicular diffusion attenuation is fitted with a baseline, which is due to restricted diffusion presumably mediated in large part by the myelin sheath. It is proposed that under conditions of relatively low permeability, the baseline parameter reflects the relative volume of IC space, and approximates this for higher permeabilities—increases in permeability decrease the applicability of the model. This analysis extends and validates the approach by Kroenke *et al.* who found that a general additive constant helped phenomenologically explain diffusion data from formalin-fixed primate brains [38].

In order to fit data, multiple *b*-values need to be acquired, although due to the time constraints of clinical DTI scans this would mean a trade-off between the number of gradient directions and number of *b*-values. The general description for a multiple gradient spin-echo diffusion experiment would be

$$S(\mathbf{g}) = S_0 \left((1 - \widehat{\mathbf{g}}' \mathbf{C} \widehat{\mathbf{g}})\, e^{-\gamma^2 \delta^2 (\Delta - \delta/3) \mathbf{g}' \mathbf{D} \mathbf{g}} + \widehat{\mathbf{g}}' \mathbf{C} \widehat{\mathbf{g}} \right) \tag{7}$$

where $\hat{\mathbf{g}}$ is the unit gradient vector.

The cylindrically symmetrical diffusion tensor **D** and the baseline tensor **C** have the same eigenvectors. Their diagonalized form is

$$\mathbf{D} = \begin{pmatrix} D_A & 0 & 0 \\ 0 & D_{\text{app}} & 0 \\ 0 & 0 & D_{\text{app}} \end{pmatrix}, \ \mathbf{C} = \begin{pmatrix} 0 & 0 & 0 \\ 0 & C_0 & 0 \\ 0 & 0 & C_0 \end{pmatrix}. \tag{8}$$

When more than one tract is suspected of populating a voxel, combinations of this approach with multitensor methods should be considered.

The model can be used to understand the MR appearance of specific pathological states of WM, although this avenue is not investigated in depth here. The most obvious example is that of cytotoxic edema that can be described as a decrease in α. The model supports the theory that the considerable reduction of apparent diffusion observed in acute stroke [35], [39] is caused by an extracellular volume decrease which increases the proximity of fibers to each other [40], [41].

Changes in parameters such as FA can potentially be better understood within this framework because more information is available. In the case of fiber tracking through areas of vasogenic edema, which can be simplistically characterized by an increase in α and spc, the fitted baseline constant C_0 may be more indicative of the existence of fibers than values derived from the diffusion tensor, which may not be extremely anisotropic.

V. CONCLUSION

A 3-D model of coherently structured tracts has been developed that allows spin packets to diffuse, relax, and exchange in a hexagonally spaced WM construction. Diffusion curves can be generated for different *b*-values, pulse sequences, gradient directions, intrinsic diffusivities, relaxivities, permeabilities and cell dimensions. Based on the model, it is proposed that multi-*b*-value DTI data be fitted by a cylindrically symmetric diffusion tensor and a cylindrically symmetric baseline tensor, effectively giving a monoexponential + baseline fit to diffusion perpendicular to the axon axis, and a monoexponential fit to the parallel diffusion. Areas of fiber crossing or bifurcation should be fit to two sets of diffusion and baseline tensors. From the fitted curves, parameters such as IC volume and extracellular tortuosity can be estimated. If the signal is measured only at lower *b*-values, it can be fit by a monoexponential, but the extracted diffusion constant will be an average of all populations, because the wrong model is being used. If higher *b*-value data is acquired, the signal can be fit to a more correct model, i.e., monoexponential + baseline, yielding far more meaningful parameters. The baseline cannot be fitted if high *b*-values are not acquired.

Results from the simulations point to the size of the extracellular compartment as an important factor influencing the signal. It affects both the apparent diffusion constant and the baseline measurement. Permeability and cell size can also impact the signal—with their influence becoming more apparent the longer the diffusing time between gradient pulses. The dependence of D_{app} and C_0 on tissue parameters is summarized in Table III.

This approach is designed to identify some of the cellular correlates of changes in measured diffusion by focusing on physiologically meaningful measures. An application of this analysis would be to enable a comparison of parcellated fiber tracts within or between subjects based on average values of tissue parameters in the tracts. The analysis could also be applied to help understand the structural correlates of disease processes in WM. The insight gained from the model could yield optimal strategies for obtaining the maximum information from DTI acquisitions, which may include combinations of different pulse sequences.

Acknowledgments

The author would like to thank the anonymous manuscript reviewers for their contributions to the completeness and accuracy of this work.

This work was funded by the National Institutes of Health under Grant R03MH076012, Grant U41RR019703, and Grant R01MH074794.

APPENDIX

RESTRICTED DIFFUSION UNDER FINITE GRADIENTS

The minimal signal attenuation of IC spins when long gradient pulses are applied is not surprising since during a gradient pulse, the mean displacement perpendicular to the tract (given by $\sqrt{4 \cdot D_A \cdot \delta}$) would be 17 μ for D_A = 2 μ^2/ms and δ = 35 ms if the diffusion was unrestricted. This means that each particle samples much of the axonal cross-sectional area during each gradient pulse, for all physiologically relevant WM axon sizes. The center-of-mass formalism developed by Mitra and Halperin explains the resulting diffusion attenuation intuitively in terms of a center-of-mass propagator [28]. Fig. 7 shows the results of simulations with larger gradient strengths than are possible *in vivo*, allowing high *q* and *b*-values with short gradient pulses. As is evident, with diffusion pulses longer than 8 ms, the simulated diffusion attenuation at b = 4 ms/μ^2, with Δ = 40 ms, is less than 1%.

REFERENCES

1. Kanaan RA, Shergill SS, Barker GJ, Catani M, Ng VW, Howard R, McGuire PK, Jones DK. Tract-specific anisotropy measurements in diffusion tensor imaging. Psychiatry Res. 2006; vol. 146(no. 1):73–82. [PubMed: 16376059]
2. Alexander AL, Lee JE, Lazar M, Boudos R, Dubray MB, Oakes TR, Miller JN, Lu J, Jeong EK, McMahon WM, Bigler ED, Lainhart JE. Diffusion tensor imaging of the corpus callosum in autism. NeuroImage. 2007; vol. 34(no. 1):61–73. [PubMed: 17023185]
3. Tuch DS, Salat DH, Wisco JJ, Zaleta AK, Hevelone ND, Rosas HD. Choice reaction time performance correlates with diffusion anisotropy in white matter pathways supporting visuospatial attention. Proc. Nat. Acad. Sci. USA. 2005; vol. 102(no. 34):12212–12217. [PubMed: 16103359]
4. Tuch DS, Reese TG, Wiegell MR, Wedeen VJ. Diffusion MRI of complex neural architecture. Neuron. 2003; vol. 40(no. 5):885–895. [PubMed: 14659088]
5. Alexander DC. Multiple-fiber reconstruction algorithms for diffusion MRI. Ann. NY Acad. Sci. 2005; vol. 1064:113–133. [PubMed: 16394152]
6. Peled S, Friman O, Jolesz FA, Westin CF. Geometrically constrained two-tensor model for crossing tracts in DWI. Magn. Reson. Imag. 2006; vol. 24(no. 9):1263–1270.
7. Bihan DL. Looking into the functional architecture of the brain with diffusion MRI. Nat. Rev. Neurosci. 2003; vol. 4(no. 6):469–480. [PubMed: 12778119]
8. Norris DG. The effects of microscopic tissue parameters on the diffusion weighted magnetic resonance imaging experiment. NMR Biomed. 2001; vol. 14(no. 2):77–93. [PubMed: 11320535]
9. Beaulieu C. The basis of anisotropic water diffusion in the nervous system—A technical review. NMR Biomed. 2002; vol. 15(no. 7–8):435–455. [PubMed: 12489094]
10. Assaf Y, Basser PJ. Composite hindered and restricted model of diffusion (CHARMED) MR imaging of the human brain. NeuroImage. 2005; vol. 27(no. 1):48–58. [PubMed: 15979342]
11. Szafer A, Zhong J, Gore JC. Theoretical model for water diffusion in tissues. Magn. Reson. Med. 1995; vol. 33(no. 5):697–712. [PubMed: 7596275]
12. Latour LL, Svoboda K, Mitra PP, Sotak CH. Time-dependent diffusion of water in a biological model system. Proc. Nat. Acad. Sci. USA. 1994; vol. 91(no. 4):1229–1233. [PubMed: 8108392]
13. Stanisz GJ, Szafer A, Wright GA, Henkelman RM. An analytical model of restricted diffusion in bovine optic nerve. Magn. Reson. Med. 1997; vol. 37(no. 1):103–111. [PubMed: 8978638]
14. Chin CL, Wehrli FW, Hwang SN, Takahashi M, Hackney DB. Biexponential diffusion attenuation in the rat spinal cord: Computer simulations based on anatomic images of axonal architecture. Magn. Reson. Med. 2002; vol. 47:455–460. [PubMed: 11870831]
15. Sen PN, Basser PJ. A model for diffusion in white matter in the brain. Biophys. J. 2005; vol. 89:2927–2938. [PubMed: 16100258]
16. Pfeuffer J, Dreher W, Sykova E, Leibfritz D. Water signal attenuation in diffusion-weighted 1H NMR experiments during cerebral ischemia: Influence of intracellular restrictions, extracellular tortuosity, and exchange. Magn. Reson. Imag. 1998; vol. 16(no. 9):1023–1032.
17. Ford JC, Hackney DB. Numerical model for calculation of apparent diffusion coefficients (ADC) in permeable cylinders—Comparison with measured ADC in spinal cord white matter. Magn. Reson. Med. 1997; vol. 37:387–394. [PubMed: 9055229]
18. Assaf Y, Cohen Y. Non-mono-exponential attenuation of water and N-acetyl aspartate signals due to diffusion in brain tissue. J. Magn. Reson. 1998; vol. 131(no. 1):69–85. [PubMed: 9533908]
19. Stejskal EO, Tanner JE. Spin diffusion measurements—Spin echoes in presence of a time-dependent field gradient. J. Chem. Phys. 1965; vol. 42:288–288.
20. Basser PJ, Mattiello J, LeBihan D. Estimation of the effective self-diffusion tensor from the NMR spin echo. J. Magn. Reson. B. 1994; vol. 103(no. 3):247–254. [PubMed: 8019776]
21. Maier SE, Vajapeyam S, Mamata H, Westin CF, Jolesz FA, Mulkern RV. Biexponential diffusion tensor analysis of human brain diffusion data. Magn. Reson. Med. 2004; vol. 51(no. 2):321–330. [PubMed: 14755658]
22. Niendorf T, Dijkhuizen RM, Norris DG, Campagne MvL, Nicolay K. Biexponential diffusion attenuation in various states of brain tissue: Implications for diffusion-weighted imaging. Magn. Reson. Med. 1996; vol. 36(no. 6):847–857. [PubMed: 8946350]

23. Sukstanskii AL, Yablonskiy DA, Ackerman JJ. Effects of permeable boundaries on the diffusion-attenuated MR signal: Insights from a one-dimensional model. J. Magn. Reson. 2004; vol. 170(no. 1):56–66.
24. Peled S, Cory DG, Raymond SA, Kirschner DA, Jolesz FA. Water diffusion, T_2 and compartmentation in frog sciatic nerve. Magn. Reson. Med. 1999; vol. 42(no. 5):911–918. [PubMed: 10542350]
25. Nicholson C. Diffusion and related transport mechanisms in brain tissue. Rep. Prog. Phys. 2001; vol. 64:815–884.
26. Basser PJ, Pierpaoli C. Microstructural and physiological features of tissues elucidated by quantitative-diffusion-tensor MRI. J. Magn. Reson. Series B. 1996; vol. 111:209–219.
27. Norris DG, Niendorf T. Interpretation of DW-NMR data: Dependence on experimental conditions. NMR Biomed. 1995; vol. 8(no. 7–8):280–288. [PubMed: 8739266]
28. Mitra PP, Halperin BI. Effects of finite gradient-pulse widths in pulsed-field-gradient diffusion measurements. J. Magn. Reson. Series A. 1995; vol. 113:94–101.
29. Van Harreveld, A. The extracellular space in the vertebrate nervous system. In: Bourne, GH., editor. The Structure and Function of Nervous Tissue. New York: Academic; 1972. p. 447-511.
30. Waxman SG, Bennett MV. Relative conduction velocities of small myelinated and non-myelinated fibres in the central nervous system. Nat. New Biol. 1972; vol. 238(no. 85):217–219. [PubMed: 4506206]
31. Friede RL, Bischhausen R. How are sheath dimensions affected by axon caliber and internode length. Brain Res. 1982; vol. 235(no. 2):335–350. [PubMed: 7188332]
32. Whittall KP, MacKay AL, Graeb DA, Nugent RA, Li DK, Paty DW. In vivo measurement of T_2 distributions and water contents in normal human brain. Magn. Reson. Med. 1997; vol. 37(no. 1): 34–43. [PubMed: 8978630]
33. Siegel, GJ., editor. Basic Neurochemistry: Molecular, Cellular, and Medical Aspects. 6th ed.. Philadelphia, PA: Lippincott-Raven; 1999.
34. Pell GS, Briellmann RS, Waites AB, Abbott DF, Lewis DP, Jackson GD. Optimized clinical T_2 relaxometry with a standard CPMG sequence. J. Magn. Reson. Imag. 2006; vol. 23(no. 2):248–252.
35. van Gelderen P, de Vleeschouwer MH, DesPres D, Pekar J, van Zijl PC, Moonen CT. Water diffusion and acute stroke. Magn. Reson. Med. 1994; vol. 31(no. 2):154–163. [PubMed: 8133751]
36. Quirk JD, Bretthorst GL, Duong TQ, Snyder AZ, Springer CS Jr, Ackerman JJ, Neil JJ. Equilibrium water exchange between the intra- and extracellular spaces of mammalian brain. Magn. Reson. Med. 2003; vol. 50(no. 3):493–499. [PubMed: 12939756]
37. Kroenke CD, Ackerman JJ, Yablonskiy DA. On the nature of the NAA diffusion attenuated MR signal in the central nervous system. Magn. Reson. Med. 2004; vol. 52(no. 5):1052–1059. [PubMed: 15508157]
38. Kroenke CD, Bretthorst GL, Inder TE, Neil JJ. Diffusion MR imaging characteristics of the developing primate brain. NeuroImage. 2005; vol. 25(no. 4):1205–1213. [PubMed: 15850738]
39. Moseley ME, Cohen Y, Mintorovitch J, Chileuitt L, Shimizu H, Kucharczyk J, Wendland MF, Weinstein PR. Early detection of regional cerebral ischemia in cats: Comparison of diffusion- and T_2-weighted MRI and spectroscopy. Magn. Reson. Med. 1990; vol. 14(no. 2):330–346. [PubMed: 2345513]
40. Sotak CH. Nuclear magnetic resonance (NMR) measurement of the apparent diffusion coefficient (ADC) of tissue water and its relationship to cell volume changes in pathological states. Neurochem. Int. 2004; vol. 45(no. 4):569–582. [PubMed: 15186924]
41. Anderson AW, Zhong J, Petroff OA, Szafer A, Ransom BR, Prichard JW, Gore JC. Effects of osmotically driven cell volume changes on diffusion-weighted imaging of the rat optic nerve. Magn. Reson. Med. 1996; vol. 35(no. 2):162–167. [PubMed: 8622579]

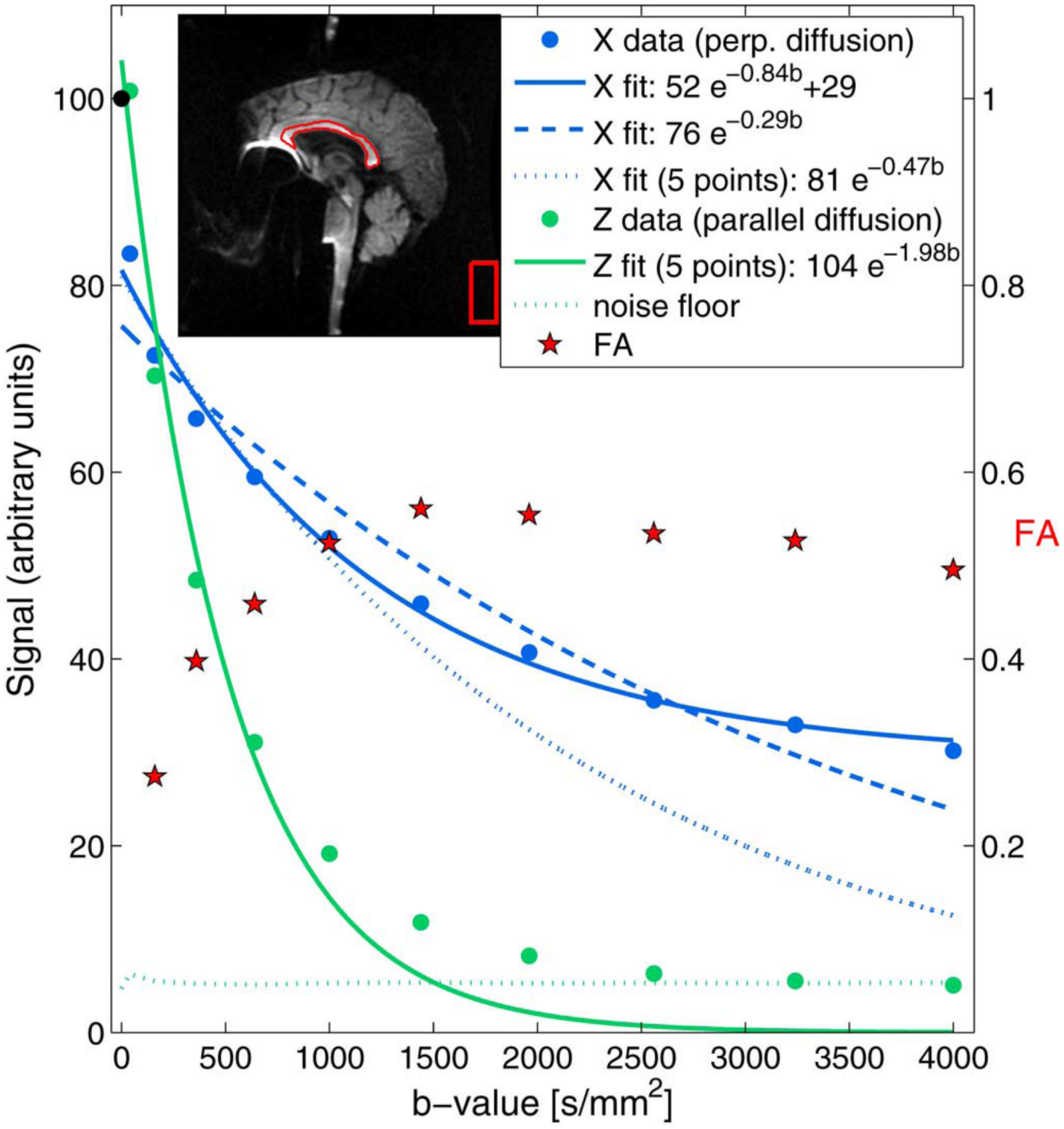

Fig. 1.

b-curves of *in vivo* transverse (blue circle), and parallel (green circle) diffusion in the corpus callosum. Perpendicular diffusion is fitted by a monoexponential (blue dashed line) to all the points, by a monoexponential to the first five points (blue dotted line), and by a monoexponential + baseline (solid blue line). Parallel diffusion is fitted by a monoexponential (solid green line). Green dotted line shows the average pixel intensity of an area of pure noise. Right *y*-axis is for the FA plot. Inset: shows outlined corpus callosum pixels that were manually selected to be averaged, and rectangular region of artifact-free background or noise calculation.

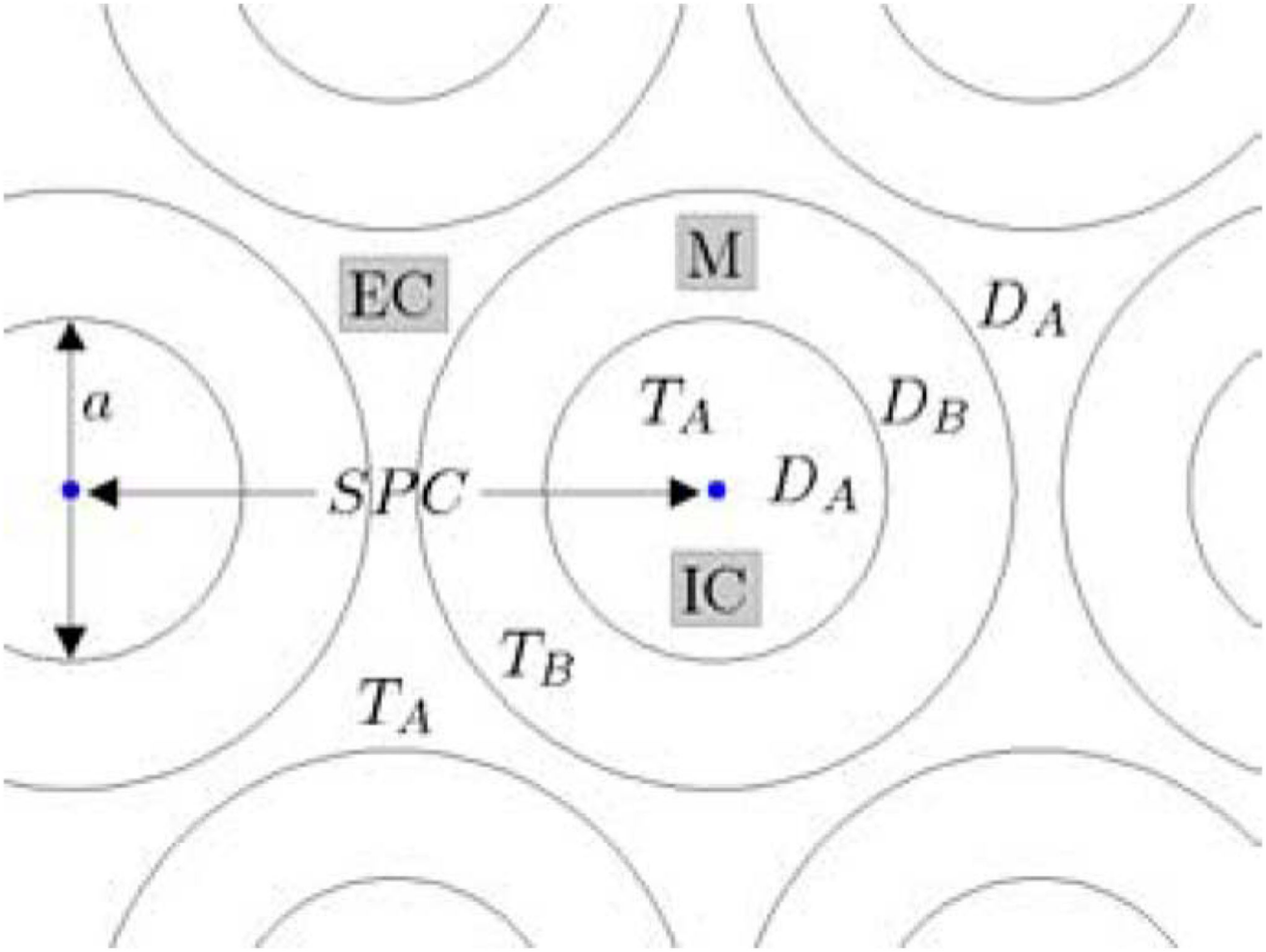

Fig. 2.
Schematic of subcellular compartments: intracellular (IC), extracellular (EC), and myelin (M), with associated model parameters.

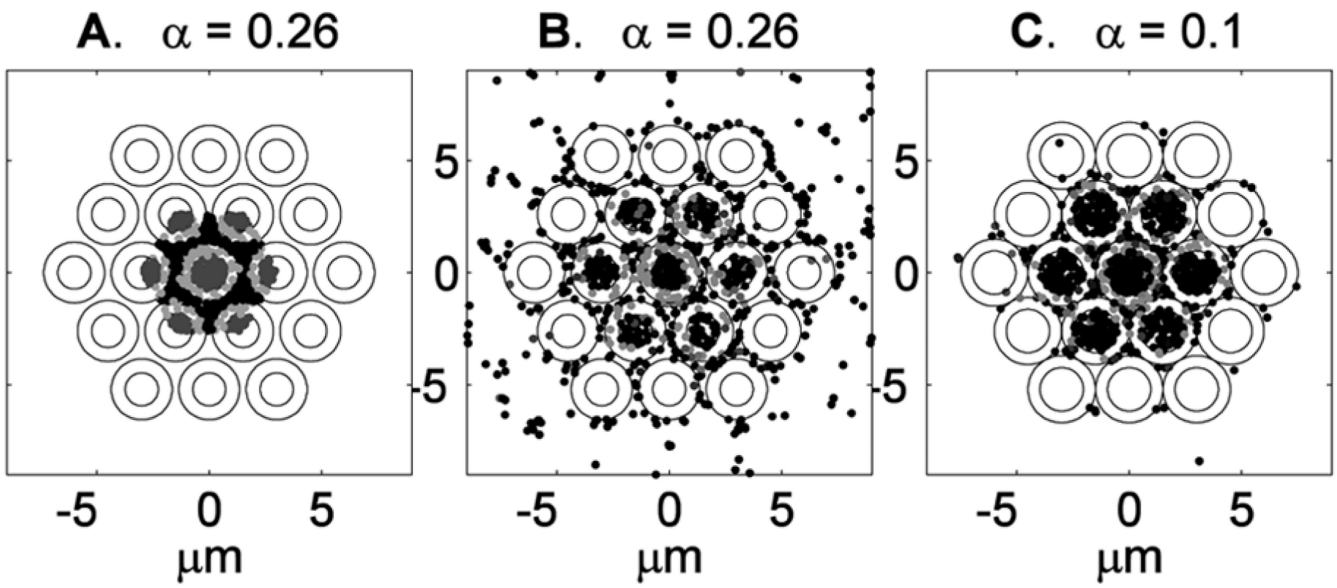

Fig. 3.

A. Initial spin placement with 26% extracellular space shaded by compartment. B. Spin location after 10 ms with 26% EC space. C. Spin location after 10 ms when EC volume is 10%. For clarity, only 1000 spins are shown out of the 10 000 used. In B. and C. spins are shaded according to relaxation experienced—the less signal remaining, the lighter.

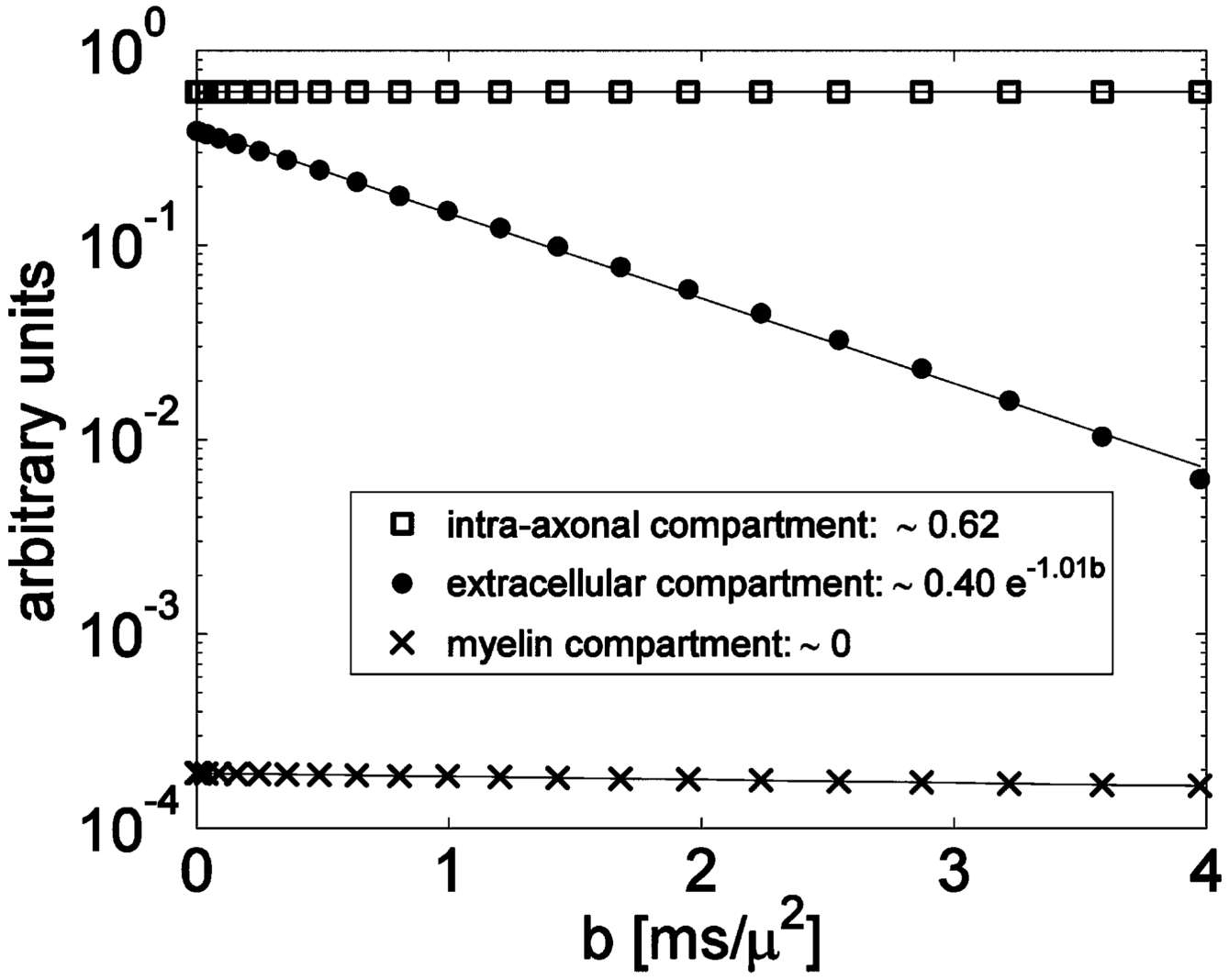

Fig. 4.
Monoexponential + baseline approximation: simulated data and fits. Data for spins in each compartment is shown separately. Permeability is zero.

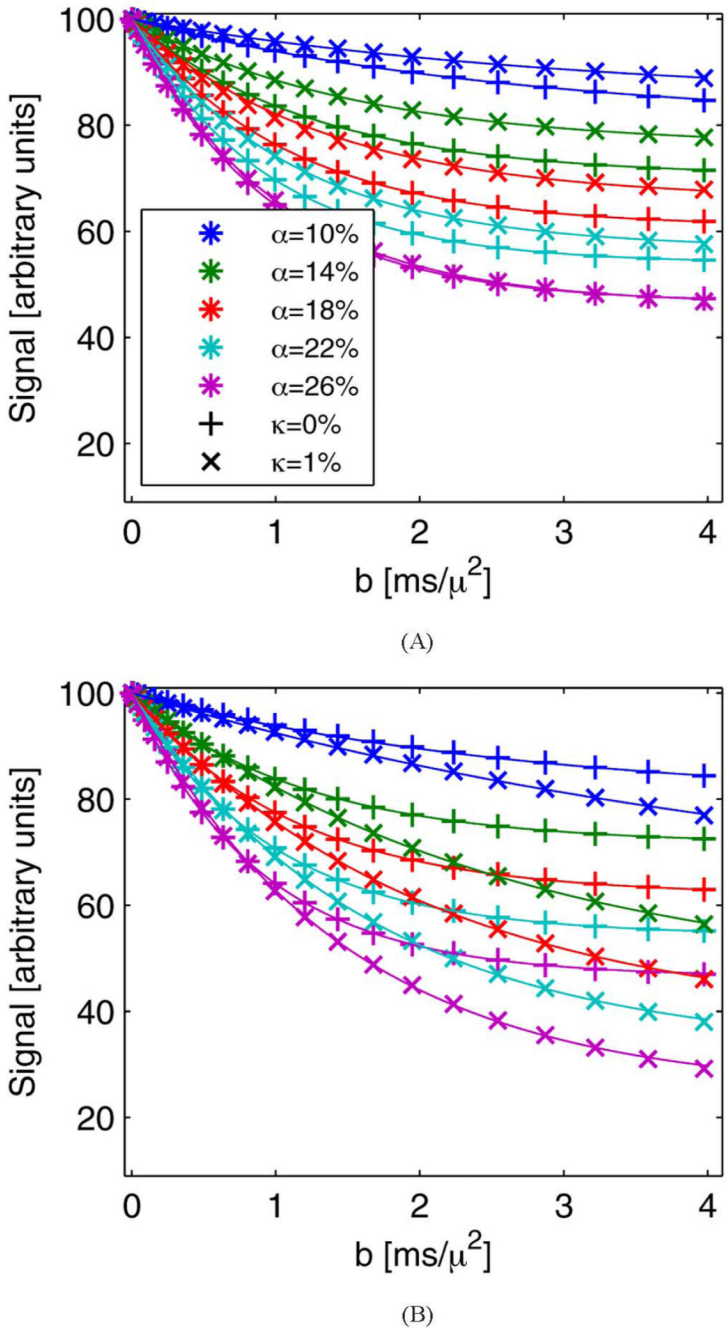

Fig. 5.

Plots of simulated data, fitted with monoexponential + baseline functions: A (top). spin echo, Δ = 40ms; B (bottom). stimulated echo, Δ = 245 ms. Other parameters: D_B = 0:5 μ²/ ms, T_B = 10 ms, spc = 6 μ.

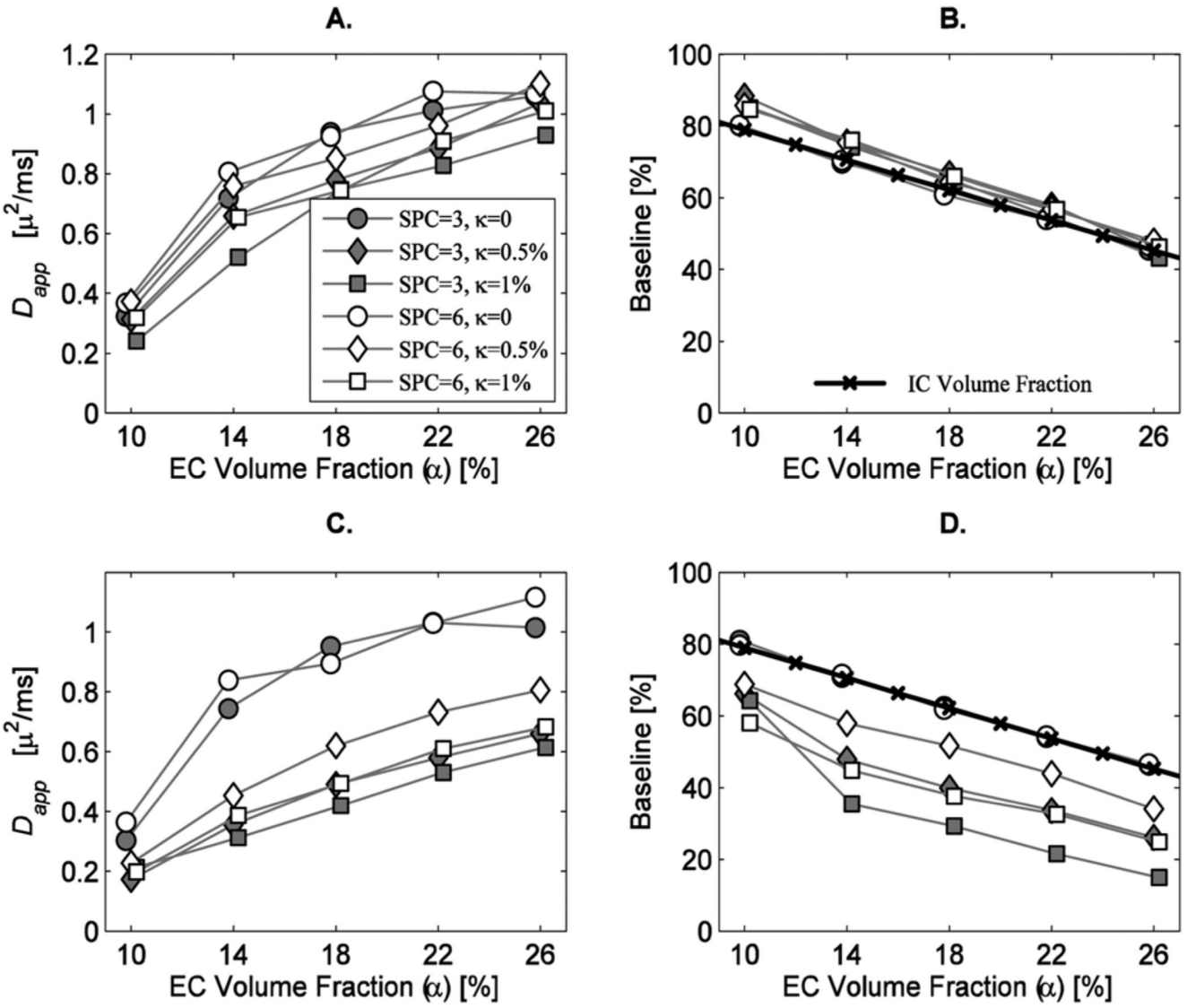

Fig. 6.

Fitted D_{app} and baseline for: A. and B. (top): spin echo, Δ = 40 ms C. and D. (bottom): Stimulated echo, Δ = 245 ms. Apparent diffusion plots are on the left; Baseline plots are on the right. The bold line of ×'s shows the relative IC volume fraction. For spc = 3 μ the axon diameter ranges from 1.5 to 1.9 μm for spc = 6 μ the axon diameter ranges from 2.9 to 3.9 μ. Other parameters, as in Fig. 5.

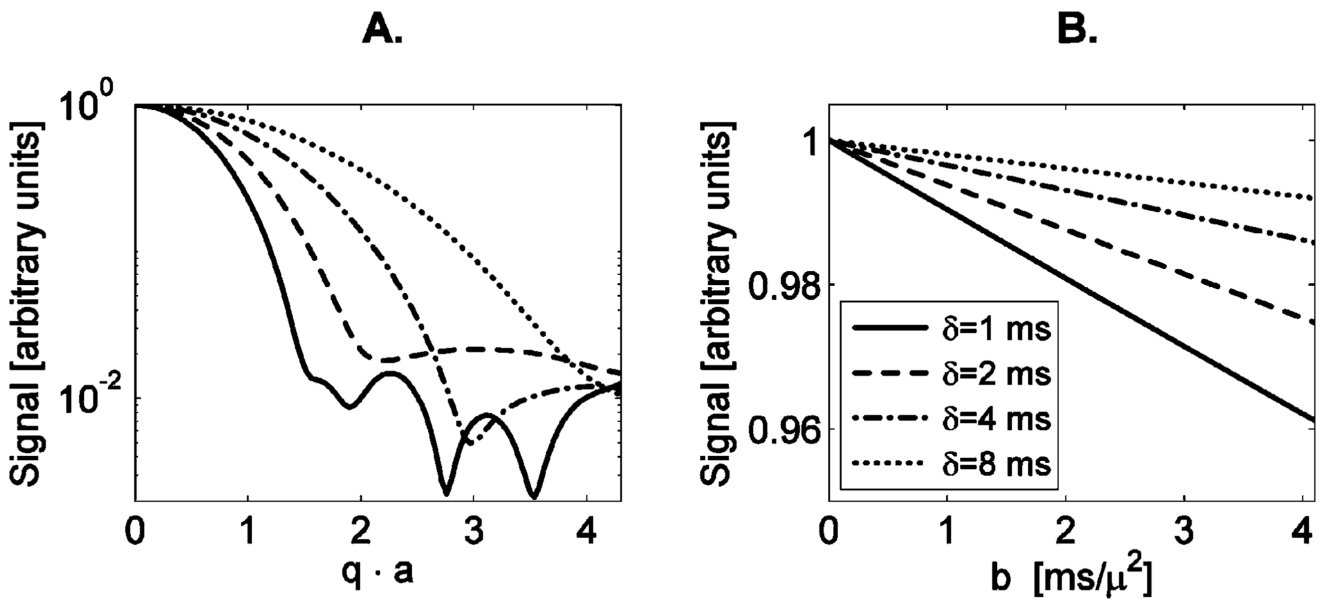

Fig. 7.

A. Simulated diffusion attenuation of the IC spins (permeability is zero) for different gradient pulse widths, δ, versus *qa*, where $q = \gamma\delta g$ and *a* is the axon diameter. B. Same diffusion attenuation plotted versus *b* at low *b*-values.

TABLE I

Model Parameters and the Range of Values Used in the Simulations

Parameter Description	Symbol	Value/s used
T_2 of IC & EC compartments	T_A	85 ms
T_2 of myelin compartments	T_B	10 ms
Diffusion coefficient of IC & EC compartments	D_A	2 μ^2/ms
Diffusion coefficient of myelin compartments	D_B	{0.5 , 2} μ^2/ms
EC volume fraction (V_{EC}/V_{WM})	α	{0.1, 0.14, 0.18, 0.22, 0.26}
Permeability: percent of wall hits that exchange	κ	{0, 0.25%, 0.5%, 0.75%, 1%}
Spacing between axon centers	SPC	{3 , 6} μ
Diffusion pulse length	δ	{35 , 12} ms
Diffusion mixing time	Δ	{40 , 245} ms

TABLE II

Different Definitions of Exchange Parameters. τ is the Average Time Before Experiencing an Exchange Event, Given By (4). Values in Parentheses are the Percent of Spins Escaping From IC to EC in TE = 75 ms

	Permeability defined by % of wall hits that exchange			
	κ=0.25%	**κ=0.5%**	**κ=0.75%**	**κ=1%**
D_B=0.5 μ^2/ms	τ=101 ms	τ=52 ms	τ=34 ms	τ=26 ms
SPC = 3 μ	(8.3%)	(15.2%)	(22.4%)	(24.8%)
D_B=0.5 μ^2/ms	τ=202 ms	τ=103 ms	τ=67 ms	τ=51 ms
SPC = 6 μ	(3.2%)	(8.3%)	(12.9%)	(15.7%)
D_B=2 μ^2/ms	τ=50 ms	T=26 ms	τ=17 ms	τ=13 ms
SPC = 3 μ	(16.5%)	(25.6%)	(29.8%)	(31.2%)
D_B=2 μ^2/ms	τ=104 ms	τ=50 ms	τ=34 ms	τ=26 ms
SPC = 6 μ	(8%)	(17%)	(22.9%)	(25%)

TABLE III

Effect of Increases in Tissue Characteristic Parameters on Fitted Elements of the Diffusion Signal

Measured value		
Tissue parameter that increases	**Apparent perpendicular diffusion: D_{app}**	**Baseline: C_0**
EC volume fraction: α	↑	↓
Permeability: κ	↓	↓
Fiber spacing: SPC	↑	↑